

Physically Derived Rules for Simulating Faceted Crystal Growth using Cellular Automata

Kenneth G. Libbrecht¹

Department of Physics, California Institute of Technology
Pasadena, California 91125

Abstract. We derive a set of algorithms for simulating the diffusion-limited growth of faceted crystals using local cellular automata. This technique has been shown to work well in reproducing realistic crystal morphologies, and the present work provides a more rigorous physical foundation that connects the numerical code to the physics of attachment kinetics and diffusion dynamics. We then apply these algorithms to examine a novel morphological transition in the growth of thin plate-like crystals.

1 Introduction

The formation of complex structures during solidification often results from a subtle interplay of nonequilibrium, nonlinear processes, for which seemingly small changes in molecular dynamics at the nanoscale can produce profound morphological changes at all scales. One popular example of this phenomenon is the formation of snow crystals, which are ice crystals that grow from water vapor in an inert background gas. Although this is a relatively simple, monomolecular system, snow crystals display a remarkable variety of columnar and plate-like forms, and much of the phenomenology of their growth remains poorly understood, even at a qualitative level [1].

Viewed broadly, snow crystal structures result from diffusion-limited crystal growth in the presence of strongly anisotropic attachment kinetics, and similar circumstances occur in a large class of solidification problems. We can break such problems down into two main physical components: 1) the attachment kinetics that describes the molecular growth dynamics at the solid surface, and 2) particle transport via diffusion to the growing crystal. In the present paper we focus on the latter problem – numerically solving the diffusion equation to model faceted crystal growth.

Computational models of diffusion-limited solidification have typically been divided into two broad camps – ‘front-tracking’ models, in which one keeps track of the solidification interface explicitly (e.g. [2, 3, 4]), and ‘phase-field’ models, in which the solidification front is numerically smoothed and not explicitly

¹e-mail address: kgl@caltech.edu; for updates on this and other papers, see <http://www.its.caltech.edu/~atomic/publist/kglpub.htm>

tracked (e.g. [5, 6]). To date, both techniques have had considerable success in modeling simple dendritic growth, but neither has been able to satisfactorily model complex morphological structures in the presence of strong faceting [7, 8, 9, 10], owing to the appearance of dynamical and numerical instabilities.

A third computation technique - local cellular automata (LCA) - has recently been applied to the problem of modeling faceted crystal growth with excellent initial success, and LCA models have produced realistic-looking snow crystal growth simulations in both 2D [11, 12] and 3D [13]. To date, however these local lattice models have incorporated largely *ad hoc* growth rules (albeit physically motivated to some extent), so the connection between the resulting simulations and real crystal growth remains tenuous. These algorithms yielded structures that bear a striking resemblance to many features seen in real snow crystals, but the similarities are largely qualitative. As a result, these models cannot be directly compared with crystal growth measurements to provide quantitative insights into growth dynamics.

The goal of this paper is to produce more accurate, physically derived rules for modeling with cellular automata, thus providing a direct connection between the numerical code and the physics of attachment kinetics and diffusion dynamics governing faceted crystal growth. The algorithms derived below provide a more rigorous physical foundation for using LCA techniques in crystal growth models. After deriving growth algorithms below for the case of snow crystal formation, we then examine the properties of the LCA model and describe a novel morphological transition seen in plate-like growth.

2 Crystal Growth Dynamics

We focus our discussion on the growth of snow crystals, as this is perhaps the most studied example of strongly faceted, diffusion-limited crystal growth. Having such a focus allows a more direct look at the relevant physics, which becomes somewhat obscured in a more general discussion. Extending the algorithms to other materials should be relatively straightforward, provided the growth dynamics are of a similar character.

We begin by assuming the "standard model" of snow crystal growth [1], for which we can first write the growth velocity normal to the surface in terms of the Hertz-Knudsen formula

$$\begin{aligned} v_n &= \alpha \frac{c_{sat}}{c_{solid}} \sqrt{\frac{kT}{2\pi m}} \sigma_{surf} \\ &= \alpha v_{kin} \sigma_{surf} \end{aligned} \tag{1}$$

where the latter expression defines the velocity v_{kin} . In this expression kT is Boltzmann's constant times temperature, m is the mass of a water molecule, $c_{solid} = \rho_{ice}/m$ is the number density for ice, $\sigma_{surf} = (c_{surf} - c_{sat})/c_{sat}$ is the supersaturation just above the growing surface, c_{surf} is the water vapor number density at the surface, and $c_{sat}(T)$ is the equilibrium number density above a flat

ice surface. The dimensionless parameter α is known as the *condensation coefficient*, and it embodies the surface physics that governs how water molecules are incorporated into the ice lattice, collectively known as the *attachment kinetics*.

The attachment kinetics can be nontrivial, so in general α will depend on T , σ_{surf} , and perhaps on the surface structure and geometry, surface chemistry, and other factors. If molecules striking the surface are instantly incorporated into it, then $\alpha = 1$; otherwise we must have $\alpha \leq 1$. The appearance of crystal facets indicates that the growth is limited in part by attachment kinetics, so we must have $\alpha < 1$ on faceted surfaces.

This model assumes that the attachment kinetics are purely local, without significant large-scale surface diffusion, especially around corners between facets. It also assumes that all complex aspects of the molecular dynamics at the ice surface, which may include surface melting and any number of other details, can be absorbed into some parameterization of α as a function of external parameters. There is currently no evidence that this "standard model" is incorrect [1], but at the same time we cannot prove that the attachment kinetics is always well described by Equation 1. For the present discussion, we will assume that this expression is valid for circumstances relevant to snow crystal growth.

Particle transport through the air surrounding a growing crystal is described by the diffusion equation

$$\frac{\partial c}{\partial t} = D \nabla^2 c \quad (2)$$

where $c(x)$ is the water molecule number density surrounding the crystal and D is the diffusion constant. The timescale for diffusion to adjust the vapor concentration in the vicinity of a crystal is $\tau_{diffusion} \approx R^2/D$, where R is a characteristic crystal size. This is to be compared with the growth time, $\tau_{growth} \approx 2R/v_n$, where v_n is the growth velocity of the solidification front normal to the surface. The ratio of these two timescales is the Peclet number, $p = Rv_n/2D$. For typical growth rates of snow crystals we find $p < 10^{-5}$, which means that diffusion adjusts the particle density around the crystal much faster than the crystal shape changes. In this case the diffusion equation reduces to Laplace's equation, $\nabla^2 c = 0$, which must be solved with the appropriate boundary conditions. Using this slow-growth limit often simplifies the problem considerably in comparison to much of the literature on diffusion-limited solidification [14].

The continuity equation at the interface gives

$$v_n = \frac{D}{c_{solid}} \left(\hat{n} \cdot \vec{\nabla} c \right)_{surf} = \frac{c_{sat} D}{c_{solid}} \left(\hat{n} \cdot \vec{\nabla} \sigma \right)_{surf} \quad (3)$$

where $\sigma(x) = [c(x) - c_{sat}]/c_{sat}$ and we are assuming the isothermal case, so c_{sat} is independent of spatial position. The latter assumption means we will be ignoring effects that arise when a growing crystal experiences a temperature increase associated with the latent heat of solidification. These effects are generally small and produce results that are similar to a simple decrease in the supersaturation surrounding the crystal [1]. Thus we believe we will not be sacrificing much interesting physics by using the isothermal approximation. We then write the

diffusion equation in terms of the supersaturation field (since c_{sat} is constant) as

$$\frac{\partial \sigma}{\partial t} = D \nabla^2 \sigma \quad (4)$$

The attachment coefficient α is not well known for ice, but on facet surfaces it appears to be well described by nucleation-limited growth [1, 15, 16], which gives

$$\alpha(\sigma) \approx A \exp(-\sigma_0/\sigma) \quad (5)$$

where A and σ_0 are parameters that depend on temperature and are different for the basal and prism facets. For growth governed by spiral dislocations, we expect [17]

$$\alpha(\sigma) \approx C\sigma \quad (6)$$

where C is independent of σ (but depends on external parameters such as temperature), which gives $v_n \sim \sigma^2$.

3 Derivation of Growth Algorithms

3.1 The 1D Problem

Because of its simplicity, it is instructive to begin with the 1D crystal growth problem, for which we assume a linear array of grid elements, or pixels, of width Δx . Each pixel is assumed to be filled with either ice or air at any given time, and each air pixel has a well-defined supersaturation $\sigma(x, t)$ associated with it. The discrete form of the 1D diffusion equation is

$$\begin{aligned} \frac{\partial \sigma}{\partial t} &= D \frac{d^2 \sigma}{dx^2} \\ \frac{\sigma(x, t + dt) - \sigma(x, t)}{dt} &= D \left[\frac{\sigma(x + dx) - 2\sigma(x) + \sigma(x - dx)}{dx^2} \right] \end{aligned} \quad (7)$$

which yields

$$\sigma(x, t + \Delta t) = \Delta\tau \sigma(x - \Delta x, t) + (1 - 2\Delta\tau) \sigma(x, t) + \Delta\tau \sigma(x + \Delta x, t) \quad (8)$$

where Δt is the physical time step in our simulation code and Δx is the grid spacing (assumed uniform). The quantity

$$\Delta\tau = \frac{D\Delta t}{(\Delta x)^2} \quad (9)$$

is a dimensionless time-step parameter. We note that $(\Delta x)^2/D$ is one natural time scale of the problem, equal the time required for diffusion to adjust the supersaturation field over a distance Δx . We define $\tau = \sum \Delta\tau$ to be the dimensionless physical time in our problem.

We use Equation 8 to effectively relax the supersaturation field to a suitable solution of the diffusion equation. Choosing $\Delta\tau$ too small will require an

excessive amount of computer time, while taking $\Delta\tau > 1$ leads to instabilities near sharp edges (*e.g.*, at physical boundaries) in σ . It appears that $\Delta\tau = 0.5$ is close to optimal, yielding the simple algorithm

$$\sigma(x, \tau + \Delta\tau) = \frac{1}{2}\sigma(x - \Delta x, \tau) + \frac{1}{2}\sigma(x + \Delta x, \tau) \quad (10)$$

for the 1D case. This expression is used to propagate σ in time for regions away from the growing crystal surface, where diffusion alone affects the particle dynamics.

Our model crystal grows as water molecules diffuse in from the outer boundaries of the system and attach to the ice surface. For boundary pixels (*i.e.*, air pixels that are adjacent to ice pixels), we see physically that the ice surface effectively "drains" the supersaturation as water vapor condenses, which in turn causes the solidification front to move with a velocity $v = \alpha v_{kin}\sigma$. This "draining" reduces the supersaturation of boundary pixels according to

$$\sigma(\tau + \Delta\tau) = \sigma(1 - \alpha\Delta\xi\Delta\tau) \quad (11)$$

where $\Delta\xi = \Delta x/X_0$ is a dimensionless pixel size in the problem and

$$\begin{aligned} X_0 &= \frac{c_{sat}}{c_{solid}} \frac{D}{v_{kin}} \\ &= D \sqrt{\frac{2\pi m}{kT}} \\ &\approx \left(\frac{D}{D_{air}} \right) (0.15 \text{ } \mu m) \end{aligned} \quad (12)$$

is the natural physical scale of the problem. Here $D_{air} = 2 \times 10^{-5} \text{ m/sec}^2$ is the diffusion constant for air at one atmospheric pressure, and the numerical value pertains to ice crystal growth.

We can combine Equation 11 with Equation 8 to create a new propagation algorithm for boundary pixels

$$\sigma(x, \tau + \Delta\tau) = \Delta\tau\sigma_{solid}(\tau) + (1 - 2\Delta\tau)\sigma(x, \tau) + \Delta\tau\sigma(x + \Delta x, \tau) \quad (13)$$

where the boundary pixel is at x and the ice pixel is at $x = x - \Delta x$, and

$$\sigma_{solid}(\tau) = \sigma(x, \tau)(1 - \alpha\Delta\xi) \quad (14)$$

With this, the same algorithm can be used for all air pixels, including boundary pixels, provided one substitutes σ_{solid} in the appropriate place for boundary pixels.

For the conversion of boundary pixels to ice, mass conservation suggests that we define an accumulated mass parameter λ that begins as $\lambda = 0$ for each air pixel. For boundary pixels, we increment λ using

$$\lambda \rightarrow \lambda + \alpha\sigma\Delta\lambda \quad (15)$$

for each time step, where

$$\Delta\lambda = \frac{c_{sat}}{c_{solid}} \Delta\tau \Delta\xi \quad (16)$$

When $\lambda \geq 1$, that pixel converts from air to ice.

For ice we have $c_{sat}/c_{solid} \approx 10^{-6}$, while the dimensionless parameters σ , $\Delta\tau$, α , $\Delta\xi$ will all be of order unity or perhaps substantially smaller. Thus it would take more than a million time steps before a boundary pixel becomes an ice pixel. This situation reflects the small Peclet number in our problem, so the growth is much slower than the time it takes diffusion to adjust the supersaturation field. We speed up the code by taking

$$\Delta\lambda = \Lambda \Delta\tau \Delta\xi \quad (17)$$

where Λ is an input constant, discussed further below.

3.2 The 2D problem in Cartesian Coordinates

Following the 1D analysis, the discrete form of the 2D diffusion equation gives

$$\sigma(\tau + \Delta\tau) = \Delta\tau [\sigma(x - \Delta x) + \sigma(x + \Delta x) + \sigma(y - \Delta y) + \sigma(y + \Delta y)] + (1 - 4\Delta\tau) \sigma \quad (18)$$

where we have dropped indices when doing so does not confuse the expression. If we take our time parameter to be $\Delta\tau = 1/4$, this becomes

$$\sigma(\tau + \Delta\tau) = \frac{1}{4} [\sigma(x - \Delta x) + \sigma(x + \Delta x) + \sigma(y - \Delta y) + \sigma(y + \Delta y)] \quad (19)$$

For boundary pixels, we again use this expression and substitute

$$\sigma_{solid} = \sigma(1 - \alpha\Delta\xi) \quad (20)$$

for each neighboring ice pixel, as with the 1D case, and we have further assumed a uniform grid with $\Delta x = \Delta y$.

We again define an accumulated mass parameter λ and increment it with

$$\lambda \rightarrow \lambda + \sum \alpha \sigma \Delta\lambda \quad (21)$$

for each time step, where the sum is over the number of ice neighbors. When $\lambda \geq 1$, that pixel converts from air to ice.

In both these expressions we must choose α with some care, as its value will depend critically on the number and orientation of neighboring solid pixels. We label a boundary pixel with (N_x, N_y) , where N_x is the number of neighboring ice pixels in the x direction and N_y is the number of ice neighbors in the y direction. Both N_x and N_y can take values 0, 1, or 2, giving nine cases for (N_x, N_y) . The cases are:

(0,0) - the pixel is an air pixel

(0,1) - one ice neighbor in the y direction, so $\alpha = \alpha_y$, the physical value appropriate for a y facet surface.

(1,0) - one ice neighbor in the x direction, so $\alpha = \alpha_x$ for an x facet surface.
(1,1) - a kink site, where the growth will not be nucleation-limited, since the corner provides a source of molecular steps. We do not know *a priori* what value to use for α on this site, but assume a constant $\alpha = \alpha_{11}$.

(0,2), (1,2), (2,0), (2,1), (2,2) - these are all unusual cases where the growth will be fast, so it shouldn't matter much what we choose for α , as long as it is large.

We can index these possibilities with a single number by computing a boundary parameter $B = 2N_x^2 + N_y^2$, where N_x is the number of x neighbors (0, 1, or 2) and N_y is the number of y neighbors. We then have $B = 0$ for an air pixel, $B = 1$ for a y facet, $B = 2$ for an x facet, $B = 3$ for a (1,1) kink location, and $B > 3$ for all other cases.

If we consider the special case where α is equal to some constant value, independent of the orientation of the surface with respect to the crystal lattice, then the growth velocity should equal $v = \alpha v_{kin} \sigma$ for all surfaces. For the (01) or (10) facet surfaces² in this constant- α case, we take $\alpha_x = \alpha_y = \alpha$, while an analysis of the growth of a (11) surface shows that we must take $\alpha_{11} = \alpha/\sqrt{2}$ if the above algorithm is to produce the correct growth velocity.

3.3 The 2D Problem in Cylindrical Coordinates

The discrete version of the Laplacian in cylindrical coordinates yields

$$\sigma(\tau + \Delta\tau) = \Delta\tau \left[\left(1 - \frac{\Delta r}{2r}\right) \sigma(r - \Delta r) + \left(1 + \frac{\Delta r}{2r}\right) \sigma(r + \Delta r) + \sigma(z - \Delta z) + \sigma(z + \Delta z) \right] + (1 - 4\Delta\tau) \sigma \quad (22)$$

where we have assumed $\partial\sigma/\partial\theta = 0$ to reduce the problem to 2D, thus yielding cylindrically symmetric crystal structures. The problem then proceeds essentially as with the 2D case in rectangular coordinates, and similar $(1 - \Delta r/2r)$ correction factors are needed for σ_{solid} and $\Delta\lambda$. With the preferred value of $\Delta\tau = 1/4$ we have

$$\sigma(\tau + \Delta\tau) = \frac{1}{4} \left[\left(1 - \frac{\Delta r}{2r}\right) \sigma(r - \Delta r) + \left(1 + \frac{\Delta r}{2r}\right) \sigma(r + \Delta r) + \sigma(z - \Delta z) + \sigma(z + \Delta z) \right] \quad (23)$$

In our model, we define the first row of pixels to have $r = 0$, for which we cannot evaluate the above expression. Instead we revert to the Cartesian form of the Laplacian to give

$$\sigma(\tau + \Delta\tau) = \Delta\tau [4\sigma(r + \Delta r) + \sigma(z - \Delta z) + \sigma(z + \Delta z)] + (1 - 6\Delta\tau) \sigma \quad (24)$$

for those pixels. If we take $\Delta\tau = 1/4$ (the same as for $r \neq 0$), this becomes

$$\sigma(\tau + \Delta\tau) = \frac{1}{4} [4\sigma(r + \Delta r) + \sigma(z - \Delta z) + \sigma(z + \Delta z)] - \frac{1}{2} \sigma \quad (25)$$

²The notation here – integers in parentheses without commas – refers to the usual Miller indices defining specific crystal surfaces. This should not be confused with our previous notation – integers in parentheses with commas – which we used to label boundary pixels.

and the negative term leads to instabilities. We could correct this by choosing a smaller $\Delta\tau$, but this would make the code run more slowly. An alternative is to use $\Delta\tau = 1/6$ for the $r = 0$ special case only, giving

$$\sigma(\tau + \Delta\tau) = \frac{1}{6} [4\sigma(r + \Delta r) + \sigma(z - \Delta z) + \sigma(z + \Delta z)] \quad (26)$$

for $r = 0$ pixels. This isn't a perfect solution, but we find it does not cause significant problems in the code, because it is only applied to a single row of pixels.

3.4 The 2D Problem in Hexagonal Coordinates

We can model planar snow crystal growth using a hexagonal lattice, which can be mapped onto a rectangular lattice as shown in Figure 1 [13]. The discrete diffusion equation becomes

$$\sigma(\tau + \Delta\tau) = \frac{2}{3} \Delta\tau \sum_{i=1}^6 \sigma_i + (1 - 4\Delta\tau) \sigma \quad (27)$$

where the index i refers to the six nearest neighbors around each pixel. For boundary pixels, we again use this expression and substitute

$$\sigma_{solid} = \sigma(1 - \alpha\Delta\xi) \quad (28)$$

for each neighboring boundary pixel, as above, and we have taken Δx to be the distance between nearest neighbors.

We again define an accumulated mass parameter λ and increment it with

$$\lambda \rightarrow \lambda + \frac{2}{3} \sum \alpha \sigma \Delta\lambda \quad (29)$$

for each time step, where the sum is over the number of ice neighbors. When $\lambda \geq 1$, that pixel converts from air to ice.

We label each boundary pixel with (N) , where N is the number of nearest neighbors:

- (0) - an air pixel
- (1) - a boundary pixel at the tip of a hexagon. The growth will be low here, and it likely doesn't matter much what value is chosen for α . The growth should be sufficient, however, to allow the crystal to grow from its initial seed.
- (2) - this case refers to the normal growth of a prism facet, and an analysis shows that we must choose $\alpha = (\sqrt{3}/2) \alpha_{prism}$ so the growth equals $v = \alpha_{prism} v_{kin} \sigma$ for this surface.
- (3) - this refers to growth at a kink site, and the choice of α here has a strong effect on the transition from faceted to branched growth [13].
- (4), (5), (6) - these are unusual cases where the growth is not much affected by the choice of α as long as it is large (of order unity).

3.5 The 3D Problem in Hexagonal Coordinates

The discrete diffusion equation becomes

$$\sigma(\tau + \Delta\tau) = \frac{2}{3}\Delta\tau \sum_{i=1}^6 \sigma_i + \Delta\tau \sum_{j=1}^2 \sigma_j + (1 - 6\Delta\tau) \sigma \quad (30)$$

where the index i refers to the six nearest neighbors around each pixel in the basal (xy) plane and j refers to the two neighbors perpendicular to this plane (the z direction). For boundary pixels, we again use this expression and substitute

$$\sigma_{solid} = \sigma(1 - \alpha\Delta\xi) \quad (31)$$

for each neighboring boundary pixel, as above. We have taken Δx to be the distance between nearest neighbors, which is the same in the basal plane as in the z direction.

We again define an accumulated mass parameter λ and increment it with

$$\lambda \rightarrow \lambda + \frac{2}{3} \sum_{i=1}^6 \alpha \sigma \Delta\lambda + \sum_{j=1}^2 \alpha \sigma \Delta\lambda \quad (32)$$

for each time step, where the sums are over ice neighbors. When $\lambda \geq 1$, that pixel converts from air to ice.

We label each boundary pixel with (N_i, N_j) , where N_i is the number of nearest neighbors in the basal plane and N_j is the number of neighbors in the z direction. We will assume that neighbors in the basal plane are contiguous. Non-contiguous cases are unusual, and it shouldn't matter much how we assign growth rates in those cases, as long as α is large.

(0,0) - an air pixel

(1,0) - a boundary pixel at the tip of a hexagon, with no z neighbors. This is similar to the case (1) in the 2D hexagonal problem above.

(2,0) - similar to the (2) case in the 2D hexagonal case above, and we take $\alpha = (\sqrt{3}/2) \alpha_{prism}$.

(3,0) - growth at a kink site, similar to the (3) case above, and again the value of α chosen will have a strong effect on the transition from faceted to branched growth [13].

(0,1) - growth of the basal facet; so we take $\alpha = \alpha_{basal}$.

(1,1) - not well determined, but faster than (1,0) or (0,1)

(2,1) - not well determined, but faster than (1,1) or (2,0)

(3,1) - again not well determined, but faster than (2,1). The values of α used for the $(N_i, 1)$ sites will strongly affect the transition from faceted growth to structure formation on the basal facet [13].

The values of α used for the remaining sites should be high, and the details will likely not affect the growth dynamics significantly.

4 Using the Algorithms

4.1 Intrinsic Anisotropies

To test our code, we modeled the growth of spherical crystals with isotropic attachment kinetics, where there is a simple analytic result for the growth rate. We limited the growth in our models to small changes in radius, to minimize non-spherical growth that eventually arises from the Mullins-Sekerka instability [17]. Our numerical model followed the prescriptions above for the 2D problem in cylindrical coordinates, with $\alpha_x = \alpha_y = \alpha = \text{constant}$ for the facet surfaces and $\alpha_{11} = \alpha/\sqrt{2}$ for a (1,1) kink site. All higher-order sites with $B > 3$ are irrelevant for this problem, because of the convex geometry of the spherical surface.

We found that our code generated growth rates that were always a few percent larger than the analytic theory for all (reasonable) choices of α , $\Delta\xi$, Λ , and other input parameters. Upon closer investigation, we found that our algorithm produces growth of a (12) surface that is approximately 8 percent faster than the (01), (10), or (11) surfaces (the latter surfaces all grow at the same rate, which, by design, is the correct rate).

This demonstrates that our choice of a fixed rectangular grid, along with only a small number of growth rules, yields an intrinsic anisotropy in the growth algorithm. This anisotropy could be reduced by adding higher-order corrections that specify slightly different α values for different boundary pixels, depending on the surface configuration beyond just the nearest neighbors, but such corrections would be difficult to implement.

This intrinsic anisotropy should not be a significant effect for strongly faceted growth, but we expect that our LCA approach would not produce accurate morphological results for cases where the anisotropy in the attachment kinetics is less than approximately 10 percent.

4.2 Scaling Behavior

If we run a growth code and produce some complex crystal shape, the interpretation of our result still contains an ambiguity. The crystal size is given in pixels, where $\Delta x = \Delta\xi X_0$ is the pixel size. The parameter $\Delta\xi$ was fixed in the code, but X_0 depends on the diffusion constant D , which is not otherwise specified. Similarly, a single time step in the code corresponds to a physical time

$$\begin{aligned}\Delta t &= \frac{(\Delta x)^2}{D} \Delta\tau \\ &= \frac{X_0^2 \Delta\xi^2 \Delta\tau}{D} \sim D\end{aligned}\tag{33}$$

Thus we see that the growth behavior at different air pressures (different D) is determined once we know the growth at a single pressure (provided σ_∞ is the same at the different pressures). If the air pressure is half an atmosphere, the

growth morphology (however complex) will be the same as at one atmosphere, except in the former case the crystal will be double the size in double the time. This scaling behavior nicely explains why snow crystal morphology is generally simpler for smaller crystals and/or for lower air pressures, which has long been observed [1]. To my knowledge, this scaling behavior has not been identified in previous investigations of snow crystal growth.

4.3 Limitations on the Grid Size

The physical size of the grid is $\Delta x = \Delta \xi X_0$, and there are limits to how coarse the grid can be without affecting the growth or causing instabilities in the code. Taking $\Delta \xi > 1/\alpha$ would cause σ_{solid} to become negative, which causes some concern in that it may produce instabilities in the code. With this limitation, the grid spacing could not be larger than $\Delta x = X_0/\alpha$. For air at a pressure of one atmosphere and $\alpha \approx 1$, this gives $\Delta x = 0.15 \mu\text{m}$. Modeling a 1.5 mm snow crystal would then require a grid with at least 10,000 pixels on a side, which is something of a computational challenge.

We can do better by realizing that a negative σ_{solid} is not itself sufficient to cause instabilities. A closer look at the algorithm reveals that problems only begin when $\sigma(\tau + \Delta\tau)$ becomes negative in a single timestep, which happens when the supersaturation is "drained" to a negative value according to Equation 11. This puts a limitation of $\Delta \xi > 1/\alpha \Delta\tau$ on the grid size, so we are able to use a coarser grid spacing if we also use a finer time step. Whatever the limit, it is important to note that our choice of grid spacing is not simply limited by a desire to produce a physically accurate model of crystal growth, but also by intrinsic instabilities in the code.

Physically, we can gain some insights into these limitations from dendrite growth theory [1]. We have $X_0 \approx R_{kin}$ (the latter from Equation 28 in [1]), and a growing dendrite has a tip radius

$$\begin{aligned} R_{tip} &= \frac{B}{\alpha s} R_{kin} \\ &\approx \frac{X_0}{\alpha s} \end{aligned} \tag{34}$$

where s is the dimensionless solvability parameter, which is of order unity for ice crystal growth [1]. The stability of the code (with $\Delta\tau \approx 1$) thus limits the grid spacing to be no greater than the tip radius of a growing dendritic structure. Interestingly, it appears that the code can only function properly when the grid spacing is fine enough to allow the growth of physically realistic dendritic structures, the scale of which is given by solvability theory.

4.4 Adaptive Time Steps

We wish to choose Λ in Equation 17 as large as possible, so the code runs quickly, while not altering the growth appreciably. Our first criterion is that the growth

be slow over a single time step, so that it takes at least $N_0 \approx 10$ time steps before a boundary pixel turns to ice, which means we must take

$$\Lambda < \frac{1}{\alpha\sigma\Delta\xi\Delta\tau N_0} \quad (35)$$

Another criterion is that the Peclet number should be small, as dictated by the physics of the growth problem, for which we find

$$\Lambda < \left(\frac{\Delta x}{R}\right) \frac{\Delta\tau}{\Delta\xi} \frac{1}{\alpha\sigma} \quad (36)$$

where R is a characteristic size of the crystal. Since $R_i = R/\Delta x$ is typically larger than N_0 , the latter requirement is the more stringent of the two.

We can speed up the code further by taking

$$\Lambda = A \frac{1}{R_{i,\max}} \frac{1}{(\alpha\sigma)_{\max}} \quad (37)$$

where $A < 1$ is a constant, $R_{i,\max}$ is the current maximum size of the crystal (in pixels), and $(\alpha\sigma)_{\max}$ is the maximum product of α and σ over all current boundary pixels. This speeds up the code considerably when the growth is strongly diffusion limited (so $\sigma \ll \sigma_\infty$) or when α is small on the crystal surface.

This choice of Λ means essentially using an adaptive time step, where the physical time for each step is equal to

$$\Delta t = \Lambda \Delta\xi^2 \Delta\tau \Delta t_0 \quad (38)$$

where

$$\begin{aligned} \Delta t_0 &= \frac{2\pi m}{kT} D \frac{c_{solid}}{c_{sat}} \\ &\approx \left(\frac{D}{D_{air}}\right) \times (1 \text{ msec}) \end{aligned} \quad (39)$$

and the latter value is for growth at $T = -15$ C [1].

5 A Morphological Transition in Plate-like Growth

We have applied the algorithms derived above to examine a key problem in snow crystal growth (and, by extension, other examples of faceted crystal growth) - understanding how small changes in extrinsic parameters like temperature and supersaturation can produce rather dramatic changes in the resulting crystal morphologies. Using our new LCA growth algorithms, we discovered an interesting example of a morphological transition in the growth of plate-like snow crystals.

We modeled the growth of small snow crystal plates in the limit of cylindrical symmetry, so we could use the 2D algorithm in cylindrical coordinates described

above. This is much simpler computationally than the full 3D problem, and the approximation is a reasonable one for small plates without dendritic branching [18]. Instead of six prism facets, the cylindrical model produces one continuous "facet" which is the perimeter of the plate. Thus, for example, hollowing of the six prism faces is replaced by hollowing of the perimeter "facet". Aside from geometrical factors of order unity, we believe the cylindrical model is a good approximation for the growth of simple plate-like snow crystals.

In our model we used a grid of $N_r = 200$ by $N_z = 100$ pixels with $\Delta\xi = 1$, corresponding to a physical grid spacing of $\Delta x = 0.15 \mu\text{m}$. The boundary condition on the $z = 0$ plane guaranteed symmetry about that plane. We began each growth run with a single ice pixel at $r = z = 0$, and we ran the code until the maximum crystal radius reached $20 \mu\text{m}$. For the basal surface, we assumed that the growth was nucleation-limited with $\alpha(\sigma) = \min[1, A \exp(-\sigma_0/\sigma)]$ with $A = 2$ and $\sigma = 0.021$, following the latest ice crystal growth measurements [16]. Accurate prism growth measurements do not yet exist, so we assumed nucleation-limited growth with $A = 5$ and $\sigma_0 = 0.01$. For non-facet surfaces we chose $\alpha_{11} = 0.7$ for the kink site with $B = 3$ and $\alpha = 1$ for all sites with $B > 3$. We believe that the morphological transition we observed is insensitive to the exact values of these growth parameters, as long as they produce plate-like structures with nucleation-limited growth on both facets.

Our results are shown in Figures 2 and 3 as we varied only the supersaturation σ_∞ in the model. The figures show a clear morphological transition from simple, thin-plate growth at low σ_∞ to concave (hollowed) growth at intermediate σ_∞ and convex growth at high σ_∞ .

The growth of thin plates at low σ_∞ (number 1 in the figures) is easy to understand from simple considerations of the growth dynamics. At low σ_∞ , α is small and the growth is largely limited by attachment kinetics, so $\sigma \approx \sigma_\infty$ at the crystal surface. The relative growth velocities of the prism and basal faces is then

$$\frac{v_{prism}}{v_{basal}} \approx \frac{A_{prism}}{A_{basal}} \exp[(\sigma_{0,basal} - \sigma_{0,prism})/\sigma_\infty] \quad (40)$$

Since $\sigma_{0,basal} > \sigma_{0,prism}$ for our case, this ratio increases rapidly as σ_∞ decreases, producing thinner plates at lower σ_∞ .

As σ_∞ increases, the higher σ values at the corners causes hollowing of both the prism and basal facets, as seen in Figure 3, number 2. For this concave growth, we see that steps are generated at the edges of the basal facets and propagate inward as the crystal grows.

As σ_∞ increases still further, the growth undergoes a rather sudden transition to convex growth, seen in Figure 3, number 3. This transition is accompanied by a reduction in crystal thickness and growth time, as seen in Figure 2. These two are related in that a thinner crystal requires less mass for a given radius, and thus grows to a given radius ($20 \mu\text{m}$ in this case) in less time. For this convex growth, steps are generated at the centers of the basal facets and propagate outward, in contrast to the concave case.

At the highest σ_∞ shown, the basal growth has increased until additional structure is seen at the center of the basal facet. Similar structures appear when

the growth rates of the prism and basal facets are comparable, and this growth behavior reflects the fact that $\alpha_{basal}/\alpha_{prism}$ increases with increasing σ_∞ as the surface values of σ begin to exceed the critical supersaturations σ_0 for the facets.

The transition from concave to convex growth as the supersaturation increases is well-known in snow crystal growth [1], because it is one of the most studied examples of faceted crystal growth. Other crystal systems may exhibit similar morphological transitions as the growth drive is increased. The morphologies that result certainly depend on the attachment kinetics, so the detailed modeling must be tailored to each individual system.

The LCA algorithms described above have proven to be quite robust and numerically stable in these calculations, while being simple to code with reasonably fast execution times. It is straightforward to change the attachment kinetics and other growth parameters to investigate different regimes. The LCA method is particularly well-suited to modeling the horizontal propagation of macrosteps on a flat surface, which appears to be a key element of faceted growth. Further studies are needed to identify whatever numerical idiosyncrasies are inherent in the LCA method (such as the intrinsic anisotropy described above), but so far it appears to be a powerful and flexible approach for modeling faceted crystal growth.

6 References

References

- [1] K. G. Libbrecht, "The physics of snow crystals," Rep. Prog. Phys. 68, 855-895 (2005).
- [2] E. Yokoyama, "Formation of patterns during growth of snow crystals," J. Cryst. Growth 128, 251-251 (1993).
- [3] E. Yokoyama and T. Kuroda, "Pattern-formation in growth of snow crystals occurring in the surface kinetic process and the diffusion process," Phys. Rev. A 41, 2038-49 (1990).
- [4] K. G. Libbrecht, "Cylindrically symmetric Green's function approach for modeling the crystal growth morphology of ice," Phys. Rev. E 60, 1967-1974 (1999).
- [5] A. Karma and W. J. Rappel, "Phase-field simulation of three-dimensional dendrites: Is microscopic solvability theory correct?," J. Cryst. Growth 174, 54-64 (1997).
- [6] R. F. Sekerka, "Morphology: from sharp interface to phase field models," J. Cryst. Growth 264, 530-540 (2004).

- [7] T. Uehara and R. F. Sekerka, "Phase field simulations of faceted growth for strong anisotropy of kinetic coefficient," *J. Cryst. Growth* 254, 251-61 (2003).
- [8] J. E. Taylor and J. W. Cahn, "Diffuse interfaces with sharp corners and facets: phase field models with strongly anisotropic surfaces," *Physica D* 112, 381-411 (1998).
- [9] J.-M. Debierre, A. Karma, F. Celestini, and R. Guerin, "Phase-field approach for faceted solidification," *Phys. Rev. E* 68, 041604: 1-13 (2003).
- [10] A. R. Roosen and J. E. Taylor, "Modeling crystal growth in a diffusion field using fully faceted interfaces," *J. Comp. Phys.* 114, 113-128 (1994).
- [11] C. A. Reiter, "A local cellular model for snow crystal growth," *Chaos, Solitons and Fractals* 23, 1111-1119 (2005).
- [12] J. Gravner and D. Griffeath, "Modeling snow crystal growth II: A mesoscopic lattice map with plausible dynamics," in press (2007).
- [13] J. Gravner and D. Griffeath, personal communication.
- [14] K. G. Libbrecht, T. Crosby, and M. Swanson, "Electrically enhanced free dendrite growth in polar and non-polar systems," *J. Cryst. Growth* 240, 241-254 (2002).
- [15] K. G. Libbrecht, "Growth rates of the principal facets of ice between -10 C and -40 C", *J. Cryst. Growth* 247, 530-40 (2003).
- [16] K. G. Libbrecht, "Precision Measurements of Ice Crystal Growth Rates," arXiv web archive paper *cond-mat/0608694* (2006).
- [17] Y. Saito, "Statistical physics of crystal growth," World Scientific (1996).
- [18] K. G. Libbrecht, "Modeling diffusion-limited crystal growth from vapor using a commercial finite-element analysis code, arXiv web archive paper *cond-mat/0610584v1* (2006).

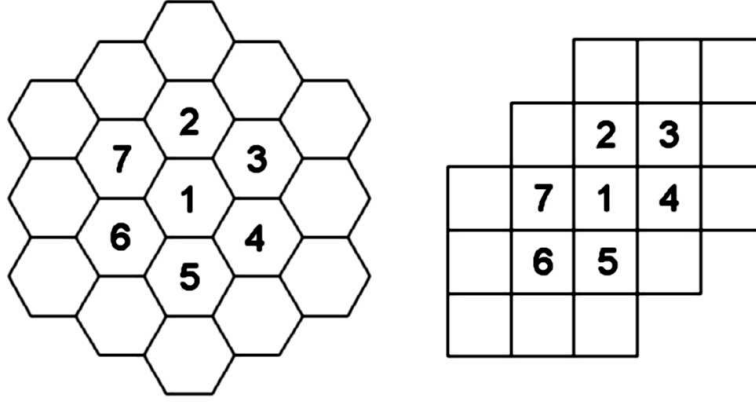


Figure 1: A mapping of a hexagonal grid onto a rectangular grid. Corresponding pixels are numbered, showing the arrangement of nearest neighbors in each case.

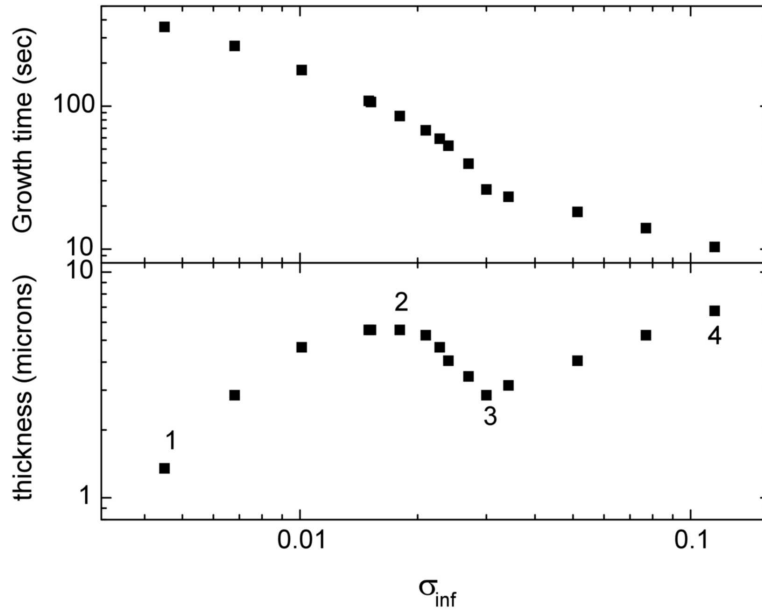


Figure 2: Modeled growth time (top panel) and final thickness (lower panel) of a crystal as a function of the supersaturation at the outer boundary. For all crystals the growth was terminated when the diameter reached $40 \mu\text{m}$. Growth parameters are described in the text. The numbers in the lower panel correspond to those in Figure 3 showing the crystal morphology.

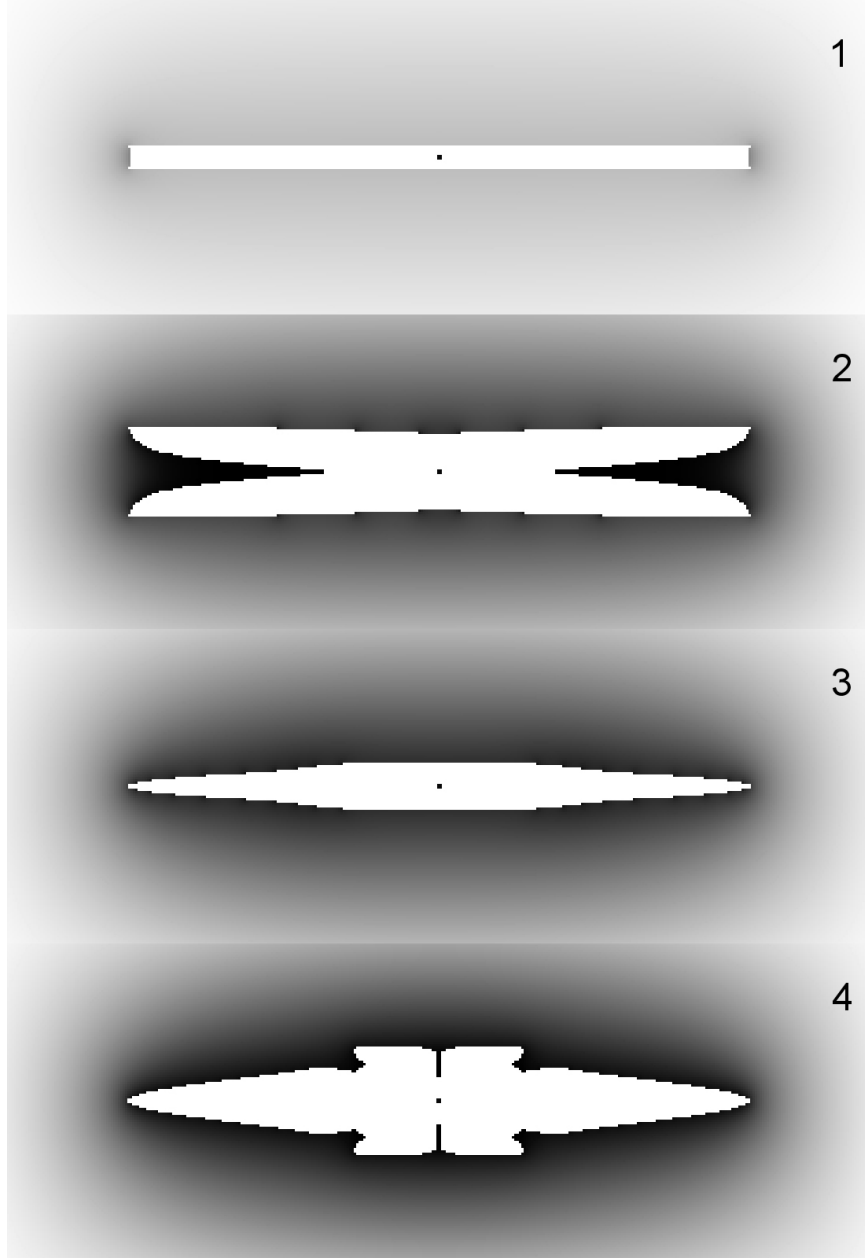


Figure 3: Full cross-sections of four plate-like crystals at the end of their growth, at which time the diameter was $40\text{ }\mu\text{m}$. The numbers beside each crystal correspond to those in Figure 2. This shows the transition from simple plate growth (1) to concave growth (2) to convex growth (3 and 4) as σ_∞ is increased.